引用格式：CHEN Yupeng, LIANG Jingqiu, LV Jinguang, et al. A Hybrid Refractive-diffractive Optical System Design for Mid-wave Infrared Interference Spectral Imaging[J]. Acta Photonica Sinica, 2026, 55(2):0222005
陈宇鹏,梁静秋,吕金光,等.中波红外干涉光谱成像折衍混合光学系统设计[J].光子学报,2026,55(2):0222005

中波红外干涉光谱成像折衍混合光学系统设计

陈宇鹏[1,2],梁静秋[1,2],吕金光[1,2],赵百轩[1,2],秦余欣[1,2],郑凯丰[1,2],赵莹泽[1,2],
聂海涛[1,2],王惟彪[1]
(1 中国科学院长春光学精密机械与物理研究所,长春 130033)
(2 光学系统先进制造全国重点实验室,长春 130033)

摘　要:中波红外干涉光谱成像仪在气体探测识别中独具优势,适配化工气体巡检预警与泄漏应急,然而传统构型在轻小型化、稳定性上局限显著,因此设计了基于阶梯微镜干涉调制的光谱成像光学系统,工作谱段为3~5 μm,F数为1.5,焦距为30 mm,视场为18°×14.4°,探测器选型为320×256像元阵列的中波制冷型探测器,通过折衍混合、非球面设计实现消色差和无热化,引入柱面镜抑制干涉分束系统导致的严重像散,为提升环境适应性保证成像质量,分析溯源视场内红外杂散辐射并进行抑制,完成样机装调后光谱成像结果显示,设计系统成像质量稳定良好且能够实现气体种类识别。

关键词:光学设计;干涉光谱成像;折衍混合;无热化;杂散辐射抑制
中图分类号:TN219　　**文献标识码**:A　　**doi**:10.3788/gzxb20265502.0222005

0 引言

红外干涉光谱成像技术因其高通量、高精度、多通道优势广泛用于航空航天、军事侦查、工业检测、安防应急等领域[1-5],尤其在化工气体日常巡检预警方面,能够在气体泄漏初期预警灾情,避免情势扩张,在气体泄漏后,在无需人员入场前提下,迅速识别泄漏气体种类和扩散浓度分布,为应急处理方案评估提供现场一手数据[6-9]。化工气体特征光谱分布于红外波段,应用场景特性对红外干涉光谱成像仪器的机动性、复杂环境适应性、视场覆盖能力和轻小型化设计提出要求,以微纳阶梯反射器件为干涉调制核心的傅里叶变换干涉光谱成像技术[10-11],其静态干涉系统的提出实现了光谱采样的高稳定性和干涉系统的轻小型化,具有应对场景变化和复杂环境的能力。除精密的干涉光谱调制系统外,成像光学系统设计亦尤为重要。

近年关于红外光学系统设计的相关报道涉及较多的均是消色差和无热化研究,中国科学院西安光机所提出了中长波红外共口径双波段成像系统,视场为中波10.1°×10.1°,长波5.1°×5.1°,在3.7~4.8 μm和7.9~9.3 μm中长波红外波段具有良好的成像质量[12];中国科学院长春光机所设计了卡式反射和透射结合的折返式制冷型中波红外系统,完成冷反射分析并进行冷反射抑制的结构优化,实现了3.7~4.8 μm中波红外波段较好性能的成像质量[13];北京空间机电研究所设计了一种－55~＋70 ℃宽温度范围内的中波红外制冷型被动消热差光学系统,视场为14.36°×10.87°,采用硅、锗等传统红外光学材料组合实现良好的成像质量[14]。

传统红外光学材料组合和构型在中波红外干涉光谱成像光学系统的无热化和轻小型化设计中具有一定的局限性,此外基于静态干涉系统的光谱成像系统设计中需解决高像散、低畸变和等相位间隔光谱采样等难题,为提升设计自由度,本文设计工作于中波红外波段3~5 μm的干涉光谱成像系统,引入衍射面通过折衍混合成像实现消色差和无热化设计,利用柱面透镜抑制平板分束器件导致的高数量级像散,凭借非球面透镜实现消像差设计,为保证前置透镜组一次成像和中继透镜组二次成像对场景的等相位间隔采样和探

基金项目:吉林省自然科学基金面上项目(20250102181JC),国家自然科学基金(62575282, 62405317, 62305339, 62205332)
第一作者:陈宇鹏,chenyp@ciomp.ac.cn
通讯作者:吕金光,jinguanglv@163.com
收稿日期:2025-11-06;**录用日期**:2025-11-27

测耦合成像匹配，设计两个透镜组分别为像方远心和物方远心光路。为适配化工气体日常巡检的复杂环境，设计红外挡光装置结合高吸收率黑体表面抑制背景红外辐射，仪器成像效果优异，能够成功捕捉到泄漏化工气体，并实现不同种类气体物质的定性识别。

1 光谱成像设计理论

本研究的干涉光谱成像系统的近似近轴光路布局如图1(a)所示，该光路布局为光谱成像系统的设计纲领，该光谱成像系统以阶梯微镜作为干涉光谱调制核心器件，与平面反射器件和分束系统共同构成基于迈克尔逊(Michelson)双干涉构型改进的静态光谱采样系统，阶梯微镜的等程差调制阶梯反射单元实现瞬态视域下的超光谱通道线阵分布采样，通过扫描反射镜实现场景扫描便可以获得全视域的光谱信息，为实现全视域的等程差间隔线阵光谱成像采样，图1(a)中的望远成像镜组设计为像方远心光路布局，与之耦合的中继成像镜组设计为物方远心，且满足冷阑匹配设计[15]。图1(b)为干涉光谱仪器的图谱处理流程，系统直接获得全视域扫描的光谱图像信息，通过干涉信息提取得到目标点的干涉强度序列，通过傅里叶变换获得目标点的光谱信息曲线。

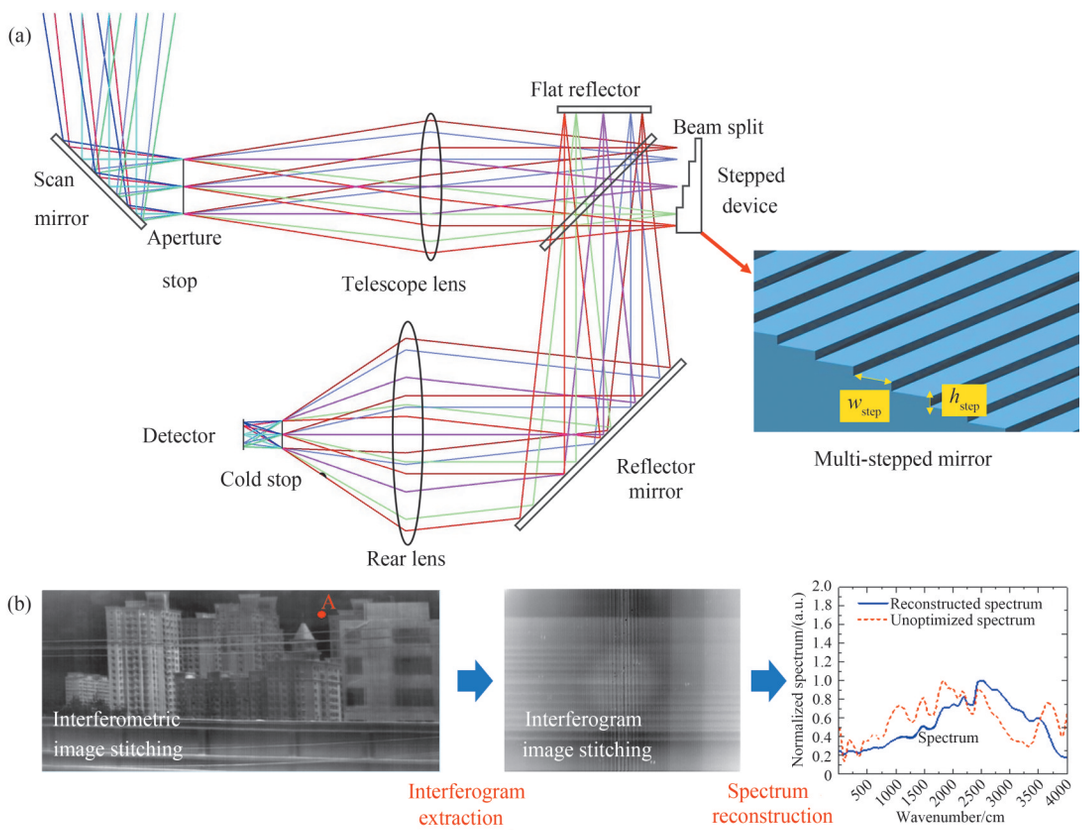


图1 干涉光谱成像系统。(a)近似近轴光路布局原理；(b)图谱处理流程

Fig. 1 Schematic diagram of the interference spectral imaging system. (a) Paraxial optical layout; (b) Imaging spectral processing flow

探测器选型碲镉汞(MCT)中波红外面阵探测机芯，像素尺寸为30 μm，像元数量为320×256，焦面尺寸为9.6 mm×7.68 mm，工作谱段范围为3~5 μm。光学系统设计指标如表1所示，设计望远成像系统的视场为18°×14.4°，一次望远成像的像面尺寸即为光谱线阵阵列尺寸，光谱线阵阵列周期数目即为光谱通道数目，与光谱分辨率成正比，为实现高光谱分辨率光谱成像系统设计，线阵周期设计为160，光谱线阵阵列尺寸为32 mm，与探测器焦面长宽比匹配，一次望远成像的像面尺寸为32 mm×25.6 mm，根据探测器焦面尺寸设计后置成像系统放大倍率为β=9.6 mm/32 mm=0.3，后置成像镜组F数F_{rear}=1.5，望远成像系统F数为$F_{Telescope}=F_{rear}/\beta$=4.5，设计望远成像系统入瞳口径为$D_{Telescope}$=22.2 mm，焦距为$f_{Telescope}=D_{Telescope}\times F_{Telescope}$=100 mm，整体系统焦距为$f_{System}=f_{Telescope}\times\beta$=30 mm。

表1 光学系统设计指标

Table 1 Optical system design specifications

Parameter	Telescope lens	Rear lens	System
Wavelength range/μm		3～5 μm	
Focal length/mm	100	75	30
Diameter/mm	22	/	22
Image space F number	4.5	1.5	1.5
Field of view	18°×14.4°	32 mm×25.6 mm	18°×14.4°
Value of MTF	>0.6@5 lp/mm	>0.5@17 lp/mm	>0.5@17 lp/mm
Distortion	<0.5%	<0.5%	<0.5%
PMAG(β)	/	−0.3×	/
Tele centricity	Image-space telecentric	Object-space telecentric	/

干涉光谱成像系统性能指标如表2所示，性能指标与阶梯微镜的结构参数直接相关，设计阶梯微镜的子阶梯单元高度为h_{step}=8.75 μm，子阶梯宽度为w_{step}=8.75 μm，总阶梯级数与线阵周期设计匹配为N_{step}=160，此时阶梯微镜的光程采样间隔为子阶梯单元高度的二倍即d_{step}=17.5 μm，最大程差为$L_{max}=N_{step}d_{step}$=160×17.5 μm=0.28 cm，光谱分辨率为$\delta\upsilon=1/L_{max}$=3.6 cm^{-1}。系统空间分辨率与系统设计焦距与成像目标物距有关，系统空间分辨率为$G_{sd}=H\times pixel/f_{System}$=2 000 m×30 μm/30 mm=2 m。本仪器对主要性能指标如光谱分辨率和空间分辨率考虑到遥测光谱成像的实际应用需求，光谱分辨率越高对气体种类识别灵敏度越高，系统设计光谱分辨率为3.6 cm^{-1}，满足各种典型气体光谱峰位分辨需求，空间分辨率2 m@2 000 m亦基本满足气体分布范围的探测需求。

表2 高光谱成像系统性能指标

Table 2 Hyperspectral imaging system performance specifications

Index parameter	Value
Spectral resolution/cm^{-1}	3.6
Spectral channel	160
Sampling interval/μm	17.5
Spatial resolution	2 m@2 000 m

本研究的干涉光谱成像系统采用折衍混合透镜和柱面透镜设计，实现消色差无热化以及消大数量级像散设计，无热化设计需满足以下条件。

光焦度分配要求为

$$\sum_{i=1}^{n}h_i\phi_i=\phi \tag{1}$$

消轴向色差要求为

$$\Delta f_b^{T}=\left(\frac{1}{h_1\phi}\right)^2\sum_{i=1}^{n}\left(h_i^{2}\omega_i\phi_i\right)=0 \tag{2}$$

无热化设计要求为

$$\mathrm{d}f_b^{T}\Big/\mathrm{d}t=\left(\frac{1}{h_1\phi}\right)^2\sum_{i=1}^{n}\left(h_i^{2}\chi_i\phi_i\right)=\alpha_h L \tag{3}$$

式中，ϕ_i为各透镜组的光焦度，ϕ为系统的总光焦度，h_i为第一近轴光线在各透镜组的高度，ω_i为各透镜组的色散因子，即色散引起光焦度的相对变化，χ_i为热差系数，即温度引起的焦距的变化率，α_h为机械结构的热膨胀系数，L为机械结构件长度。

衍射面基于光场衍射理论，在传统光学表面片基上刻蚀产生多个台阶的浮雕结构或连续浮雕结构，形成同轴环带结构，衍射光学器件焦距是由中心波长和环带半径决定的，r_m为第m个环带半径，f_m为第m个环带焦距，则为

$$f_m=\frac{n_0 r_m}{2m\lambda_0} \tag{4}$$

式中，n_0为介质折射率，λ_0为中心波长。

折射器件的热差系数为

$$\chi_{f,r}=\frac{1}{f}\frac{\mathrm{d}f}{\mathrm{d}T}=\alpha_g-\frac{1}{n-n_0}\left(\frac{\mathrm{d}n}{\mathrm{d}T}-n\frac{\mathrm{d}n_0}{\mathrm{d}T}\right) \tag{5}$$

衍射器件的热差系数为

$$\chi_{f,d}=\frac{1}{f}\frac{\mathrm{d}f}{\mathrm{d}T}=2\alpha_g+\frac{1}{n_0}\frac{\mathrm{d}n_0}{\mathrm{d}T} \tag{6}$$

式中，f为焦距，α_g为光学材料的热膨胀系数，n为光学材料的折射率，T为环境温度，$\mathrm{d}n/\mathrm{d}T$为材料的温度折射率系数，$\mathrm{d}n_0/\mathrm{d}T$为介质的温度折射率系数。可知折射器件的温度特性由材料的热膨胀系数和材料的温度折射率系数决定，而衍射器件的温度特性只由材料的热膨胀系数决定，此外折射器件的热差系数和衍射器件的热差系数符号相反，将两者合理组合，相互补偿达到消热差目的。

2 设计结果

分束系统引入大数量级像散导致弧矢和子午成像离焦，为抑制像散在前置望远成像镜组和后置中继成像镜组中均引入柱面型设计透镜，提高柱面型装调自由度，设计柱面分别位于前置望远成像镜组的最终光学表面和后置中继成像镜组的第一光学表面。为减小镜组镜片数量，提高轻量化和光透过率，设计采用高阶偶次非球面设计，非球面表达式为

$$z=\frac{cr^2}{1+\sqrt{1-(1+k)c^2r^2}}+Ar^2+Br^4+Cr^6+Dr^8+\cdots \tag{7}$$

式中，c为非球面定点的曲率半径；k为圆锥系数(Conic)；r为归一化半径坐标；A、B、C、D分别为二次项、四次项、六次项和八次项的非球面系数，设计中优化了四次项、六次项、八次项和十次项作为优化变量。表3为系统设计中各偶次非球面的圆锥系数和高阶非球面系数。

表3 系统中各偶次非球面的圆锥系数和高阶非球面系数

Table 3 High order aspheric coefficients and conic index of all the even aspheric surfaces in the system

Aspheric coefficient	2nd lens of pre-imaging	3rd lens of pre-imaging	3rd lens of relay imaging	4th lens of relay imaging
Conic	0	3.588	−1.546	7.683
4th order term	4.927×10^{-6}	-1.833×10^{-6}	-2.257×10^{-7}	2.142×10^{-6}
6th order term	-1.01×10^{-10}	1.365×10^{-10}	-1.65×10^{-11}	1.259×10^{-10}
8th order term	1.372×10^{-12}	-3.999×10^{-13}	-7.809×10^{-16}	4.388×10^{-12}
10th order term	-1.834×10^{-15}	-1.481×10^{-16}	-1.801×10^{-18}	-4.388×10^{-15}

设计前置成像镜组为像方远心光路，采用四片式结构，选型光学材料分别为硅、锗、锗和硅，第二透镜采用偶次非球面设计，第四透镜采用柱面型设计，优化后光路布局如图2所示。

图3为前置望远成像镜组在一次像面的各视场像点分布，探测器像元尺寸为p=30 μm，在一次像面处的像元投影尺寸为$p/|\beta|$=30 μm/0.3=100 μm，即在一次像面处前置成像镜组的像点点列尺寸小于100 μm

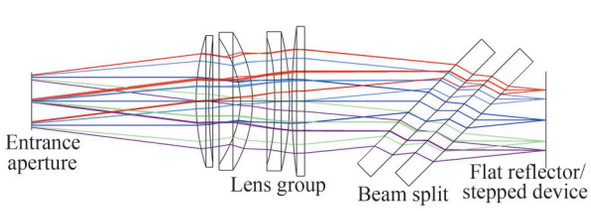


图2 干涉光谱成像系统前置望远成像镜组布局

Fig. 2 Layout of the fore-optics for an interference spectral imaging system

即可，图3中的像点尺寸均方根（Root Mean Square，RMS）值均小于58.2 μm，满足成像最小空间分辨需求，优化后的前置成像镜组的出瞳距为6 200 mm，具有高像方远心度。

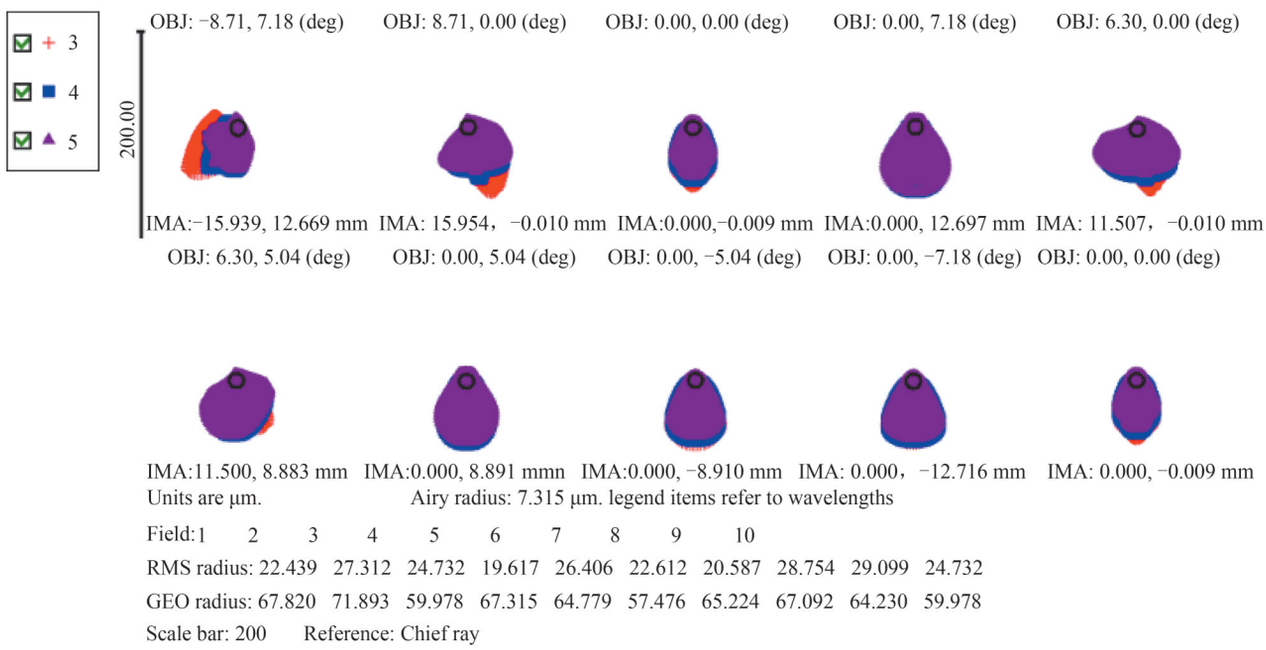


图3 前置望远成像镜组在一次像面的各视场像点分布

Fig. 3 Image spot distribution for different fields at the primary image plane

设计后置中继镜组为物方远心光路以便与前置成像镜组光路匹配，采用五片式结构，选型光学材料分别为硅、硅、锗、硅和硒化锌，对锗镜设计二元衍射面，相位函数为式（8），衍射系数设计值为二阶，分别为$A_1=-2\,388.417$，$A_2=1\,379.507$，ρ为归一化的径向孔径坐标，优化后光路布局如图4所示。

$$\phi(\rho)=2\pi\left(A_1\rho^2+A_2\rho^2+\cdots\right) \tag{8}$$

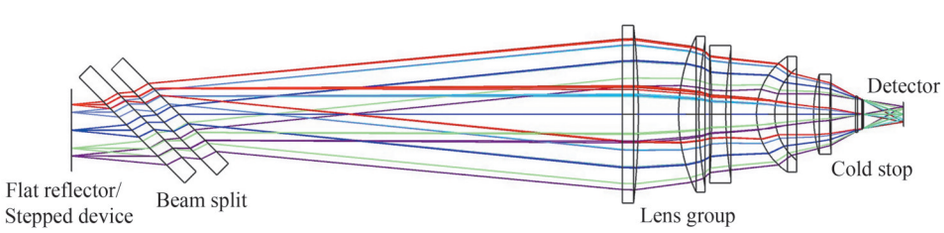


图4 干涉光谱成像系统中继成像镜组布局

Fig. 4 Layout of the relay-optics for an interference spectral imaging system

优化后的后置中继镜组入瞳距为-8 900 mm，足以与前置成像镜组进行远心匹配，为压缩体积实现光学系统的紧凑化设计，引入折转反射镜将前置成像镜组与后置中继镜组进行匹配优化，如图5所示为整体干涉光谱成像系统光路布局，图6所示为光谱成像系统的像质评价，（a）为整体传函（Modulation Transfer Function，MTF），设计静态传函在截止频率处优于0.8@17 lp/mm，（b）为系统畸变＜0.2%，（c）为成像点列RMS半径小于5.9 μm，直径尺寸远小于单像元30 μm，像质均满足设计指标要求。

对干涉光谱成像系统在宽温差范围内进行无热化系统设计，镜筒等结构材料选型为铝材，其线膨胀系数为23.6×10^{-6}/K，多重热结构下的无热化优化后在-40～60 ℃宽温差范围内的传函均满足成像需求，在各温度环境下截止频率处传函均满足MTF@17 lp/mm＞0.7。

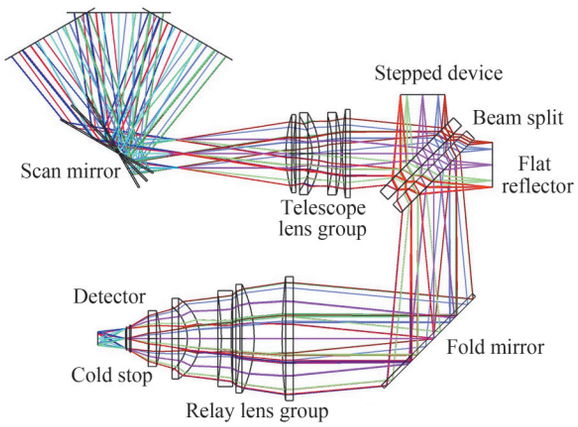


图5 整体干涉光谱成像系统光路布局

Fig. 5 Layout of the overall system for an interference spectral imaging system

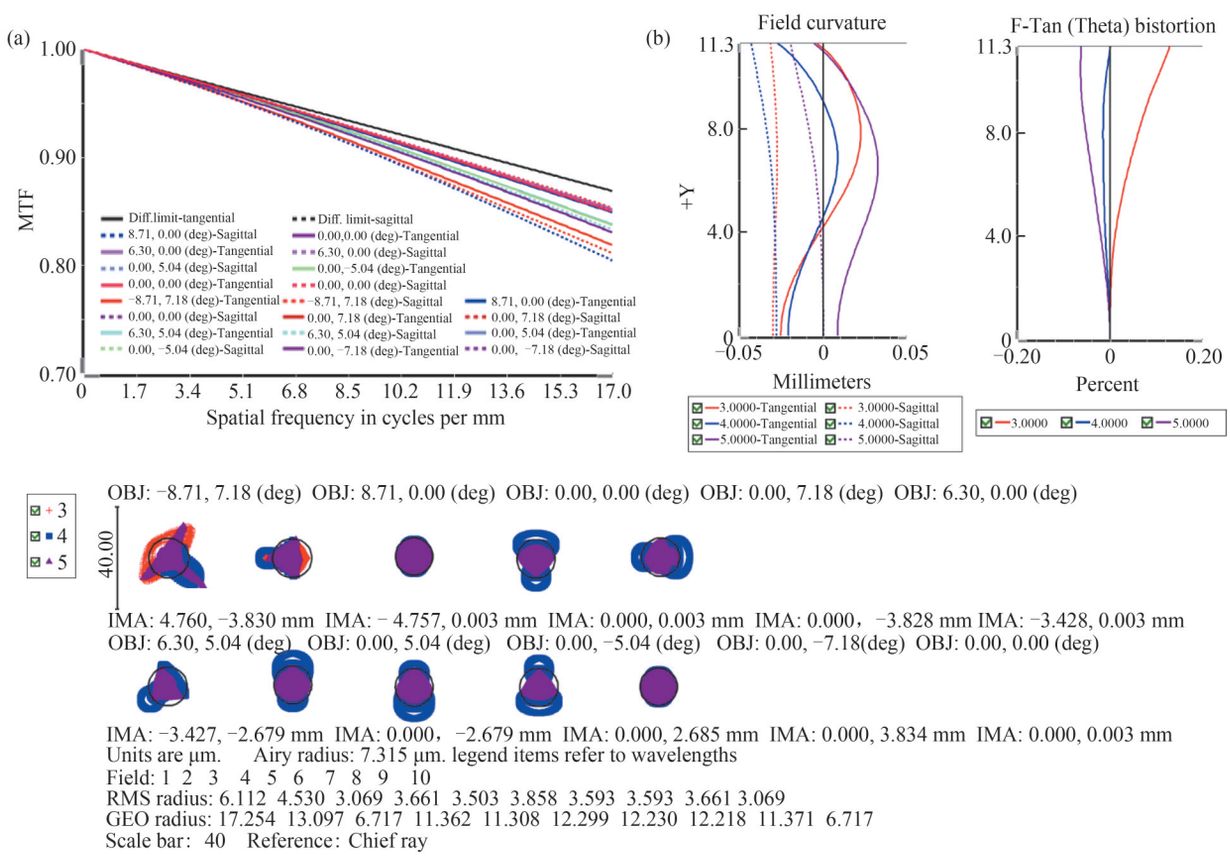


图6 干涉光谱成像系统像质评价。(a)传递函数;(b)场曲和畸变;(c)像面点列图分布

Fig. 6 Image quality evaluation of interference spectral imaging system. (a) Transfer function; (b) Field curvature and distortion; (c) Distribution of image spots

3 系统分析实验

3.1 红外杂散辐射分析与抑制

为保证光谱反演精度,干涉光谱成像系统对焦面杂散辐射能量提出严格要求,杂散辐射能量主要分为两部分,其一是扫描镜窗口易导致孔径光阑外红外辐射进入仪器内部,经内部光机结构多次反射入射到红外探测焦面,其二是光机结构自红外辐射同样有进入红外探测焦面的几率。为分析红外杂散辐射影响,构建干涉光谱成像系统杂散辐射仿真模型,设置光机结构的材料和辐射散射特性,如图7所示为杂散辐射光线追迹路径。

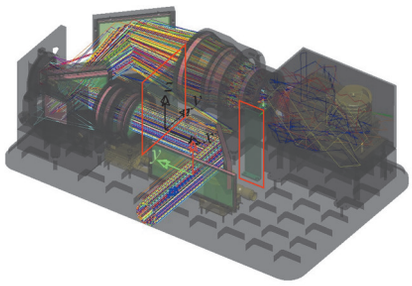


图7　杂散辐射光线追迹路径

Fig. 7　Stray radiation ray tracing path

对成像视场内各视场的红外辐射进行干涉光谱成像系统内部辐射传递仿真，如图8所示分别为对(0°，0°)、(3°，0°)、(6°，0°)、(9°，0°)、(0°，2°)、(0°，4°)、(0°，6°)、(3°，2°)和(6°，4°)等成像视场入射光在探测焦面上的辐射分布。杂散辐射照度总能量范围为0.39～3.57 W，与成像辐射照度比分别为1.54%、7.54%、1.53%、2.62%、2.62%、1.39%、1.19%、1.35%、0.84%。该数量级红外杂散辐射将严重影响成像质量和光谱重构精度，因此对主要杂散辐射照度进行单光束追迹溯源，发现成像视场内主要杂散辐射来源于两部分，其一是源于扫描长窗口直接入射到折转反射镜上，进而经后置中继成像系统无规则会聚到探测焦面上；第二部分源于扫描长窗口直接入射到后置中继系统的末端机械结构上并反射至探测焦面上。

为抑制主要杂散辐射，设计红外挡光板防止这两部分杂散辐射通过扫描长窗口直接进入探测焦面，同时对光机结构表面进行高吸收率黑化处理，抑制多次反射和高阶散射。

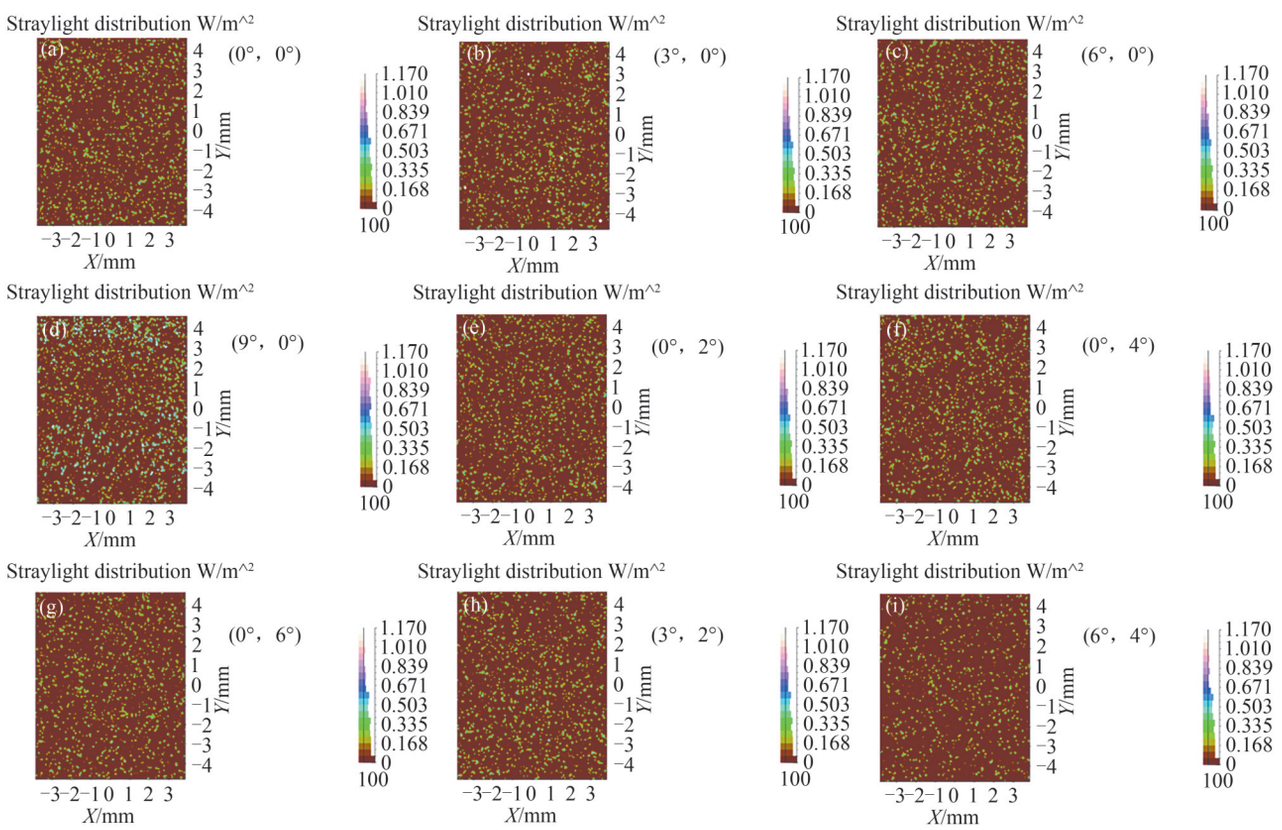


图8　各个视场入射光在探测焦面上的杂散红外辐射分布

Fig. 8　Distribution of stray infrared radiation from incident light of different fields of view on the focal plane

设计红外挡光装置结合高吸收率黑体表面实现视场内红外辐射抑制，如图7中标记部分即为红外挡光装置，对光机结构表面均匀涂敷红外高吸收率漆面，使其对红外杂散辐射吸收率优于92%，如图9所示，在该消光抑制和表面处理的设计下，辐射仿真追迹结果显示在探测焦面上杂散辐射照度总能量范围降低到

0.000 89～0.002 3 W，与成像辐射照度比分别为0.003 2%、0.004 8%、0.005 1%、0.002 4%、0.003 8%、0.001 9%、0.003 8%、0.004 1%、0.002%。如图10所示为设计红外挡光装置结合高吸收率黑体表面前后的杂散辐射照度比，杂散辐射分析抑制后，杂散辐射能量比处于10^{-5}量级，满足成像和光谱反演要求。

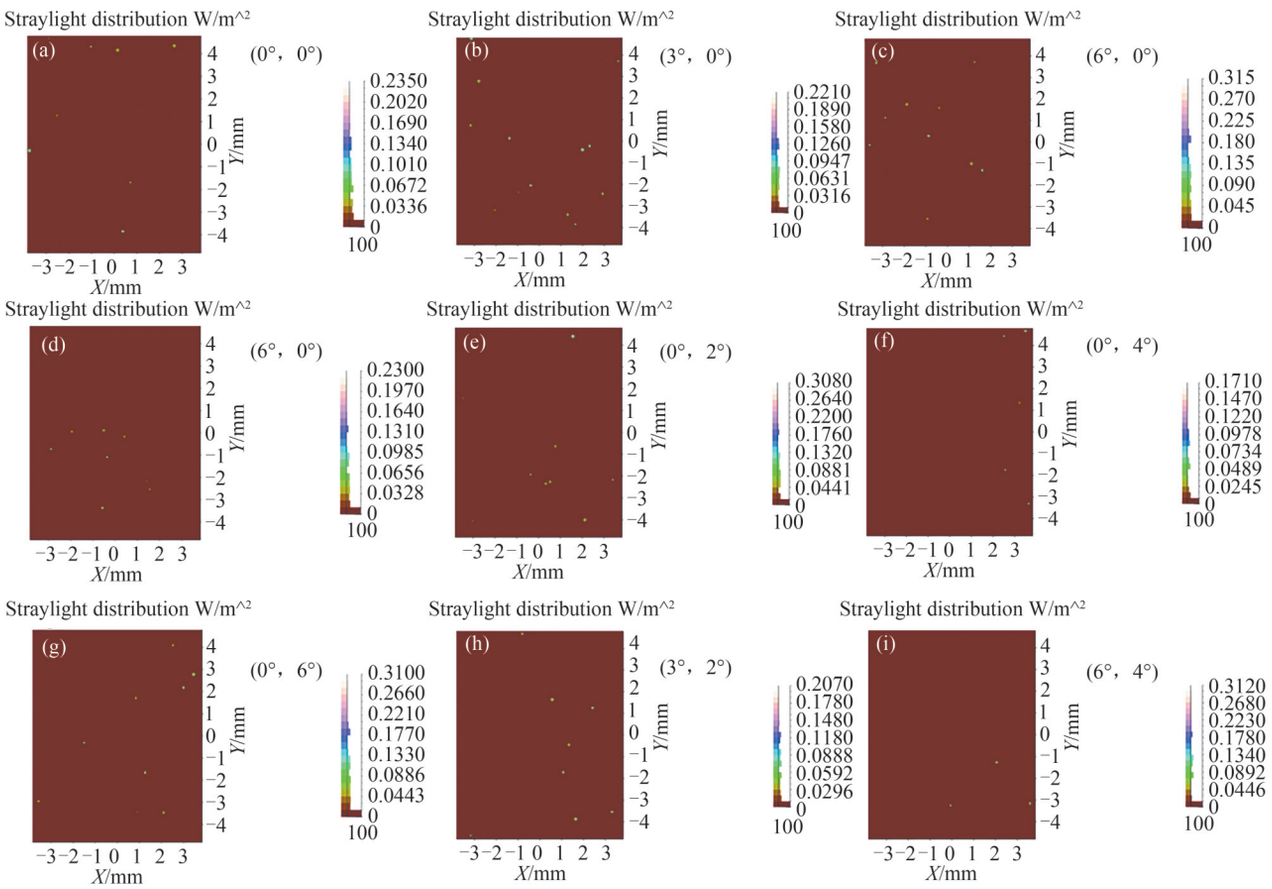


图9 抑制设计后的各个视场入射光在探测焦面上的杂散红外辐射分布

Fig. 9 Distribution of stray infrared radiation from incident light of different fields of view on the focal plane after stray radiation suppression design

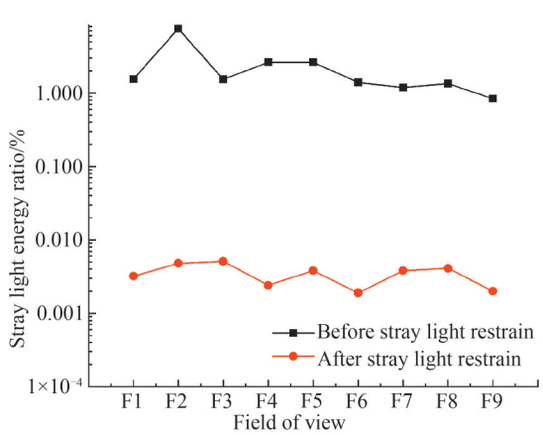


图10 抑制设计前后的各个视场入射光在探测焦面上的杂散红外辐射分布对比

Fig. 10 Distribution contrast of suppressed stray infrared radiation from incident light of different fields of view on the detection focal plane before and after stray radiation suppression design

3.2 成像实验

对中波红外干涉光谱成像仪器进行高精度装调，在实验室环境下对系统的传递函数MTF进行测试，利用半月型靶标作为MTF测试目标，如图11(a)为测试成像结果，半月型靶标边缘成像对比度较高。取红色

框选明暗过渡的有效区域利用刀口法计算实测成像传递函数，对框选区域内在垂直边缘方向上对多行数据求均值得到边缘扩展函数（Edge Spread Function，ESF）如11(b)所示，然后利用边缘扩展函数与线扩展函数的微分关系计算得到线扩展函数（Line Spread Function，LSF）如11(c)所示，最终通过傅里叶变换得到调制传递函数MTF如11(d)所示。给出的MTF截止角频率为0.5 cycle/mrad，截止角频率通过成像系统的中心波长、焦距、F数、探测像元尺寸计算得到，在成像系统截止角频率处的测试MTF为0.32，测试结果表明成像系统的传函满足设计要求。

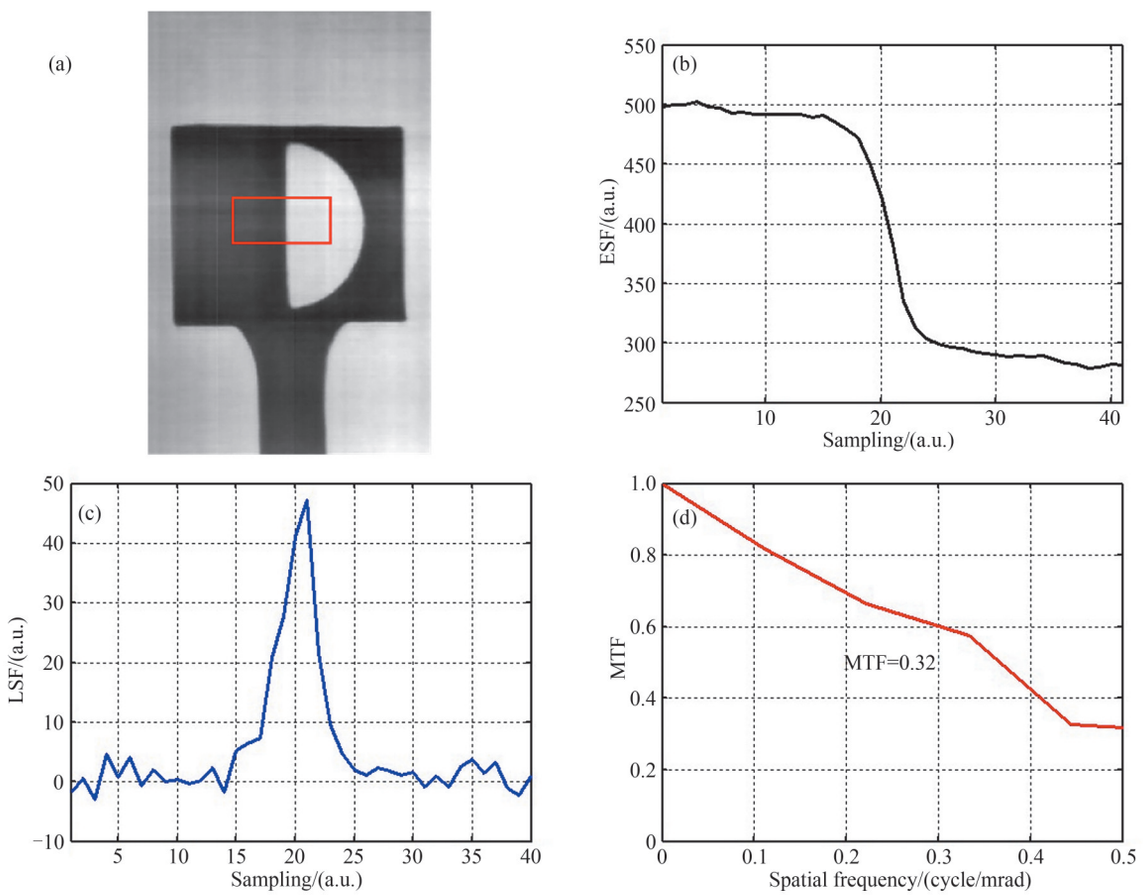


图11　光学成像系统MTF测试结果。(a) 半月型靶标探测成像；(b) 边缘扩展函数；(c) 线扩展函数；(d) 实测传递函数

Fig. 11　MTF test results of optical imaging system. (a) Half-moon target detection imaging; (b) Edge spread function; (c) Line spread function; (d) Measured transfer function

利用原理样机对远距离高温烟羽排放目标场景进行扫描成像实验，获得结果如图12所示[16]。原理样机体积仅为400 mm×200 mm×200 mm，质量仅为12.5 kg，样机对泄漏化工气体进行实时捕获，成像清晰，并

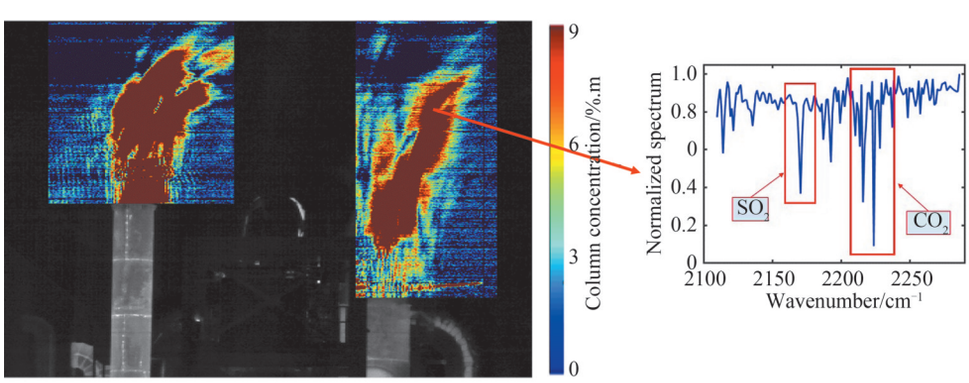


图12　干涉光谱成像仪器成像实验结果

Fig. 12　Imaging experimental results of interference spectral imaging instruments

对其光谱进行重构分析，图12中可以看到通过重构光谱曲线能够定性识别出高温烟羽中存在二氧化硫(SO_2)气体和二氧化碳(CO_2)气体排放，实验结果验证干涉光谱成像仪器样机能够实现高质量遥测成像和目标光谱的定性识别。

4 结论

本文对应用于化工气体泄漏监测的中波红外干涉光谱成像系统进行了光学设计与杂散辐射分析，采用折衍混合光学透镜、非球面透镜和柱面透镜实现了消色差、抑制像散、无热化设计，实现了3～5 μm中波红外谱段大视场、高静态传函、低畸变、紧凑型化设计，并进行了红外杂散辐射分析。仿真因扫描长窗口引入的杂散辐射和多次高阶反射散射会聚在探测焦面上的杂散辐射照度，并设计红外挡光装置结合高吸收率黑体表面实现视场内红外辐射抑制，将杂散辐射照度比降低了三个数量级，使其低至10^{-5}量级，满足中波红外成像设计需求，仪器体积降低四分之一，质量降低60%左右，对高精度装调原理样机进行MTF测试，测试表明设计成像系统实际MTF在截止频率处优于0.32，并利用仪器样机对远距离高温烟羽排放气体目标进行遥测实验，结果表明红外成像质量清晰优异，并成功对排放气体实现了精准的定性识别。

参考文献

[1] HU Bingliang. Review of the development of interferometric spectral imaging technology (invited)[J]. Acta Photonica Sinica, 2022, 51(7): 0751401.
胡炳樑.干涉光谱成像技术发展的回顾(特邀)[J].光子学报, 2022, 51(7): 0751401.

[2] SONG Siyuan, GAO Bo, WANG Shuai, et al. Mid-wave infrared snapshot spectral imaging via spectral reconstruction [J]. Acta Photonica Sinica, 2025, 54(8):0811001.
宋思远,高博,王帅,等.基于光谱重构的中波红外快照型光谱成像技术研究[J].光子学报,2025,54(8):0811001.

[3] TSAI C Y, HONG C, HSU M Y, et al. Fluorescence-based reagent and spectrum-based optical reader for lactoferrin detection in tears: differentiating Sjögren's syndrome from non-Sjögren's dry eye syndrome[J]. Scientific Reports, 2024: 14: 14505.

[4] SHANG S, LEE Z, LIN G, et al. Sensing an intense phytoplankton bloom in the western Taiwan Strait from radiometric measurements on a UAV[J]. Remote Sensing of Environment, 2017, 198: 85-94.

[5] LI Tianjiao, ZHANG Chuanxin, LIU Dong. Simultaneously retrieving of soot temperature and volume fraction in participating media and laminar diffusion flame using multi-spectral light field imaging[J]. International Journal of Thermal Sciences, 2023, 193: 108472.

[6] PHINN S, ROELFSEMA C, DEKKER A, et al. Mapping seagrass species, cover and biomass in shallow waters: an assessment of satellite multi-spectral and airborne hyper-spectral imaging systems in Moreton Bay (Australia) [J]. Remote Sensing of Environment, 2008, 112 (8): 3413-3425.

[7] BING Z, WEI Y, GAO L, et al. Real-time target detection in hyperspectral images based on spatial-spectral information extraction[J]. Eurasip Journal on Advances in Signal Processing, 2012, 2012: 142.

[8] SHANG S, LEE Z, LIN G. Sensing an intense phytoplankton bloom in the western Taiwan Strait from radiometric measurements on a UAV[J]. Remote Sensing of Environment, 2017, 198: 85-94.

[9] YUAN Pan, TAN Zhuyan, ZHANG Xu, et al. Research on infrared imaging detection and differential spectrum filtering detection methods for industrial gas leakage[J]. Infrared and Laser Engineering, 2022, 51(8): 20210714.
袁盼,谭竹嫣,张旭,等.工业气体泄漏红外成像检测及差分光谱滤波检测方法研究[J].红外与激光工程,2022,51(08): 20210714.

[10] JinguangLÜ, LIANG Jingqiu, ZHAO Baixuan, et al. Interference modulated fourier transform spectral imaging technology (invited)[J]. Acta Optica Sinica, 2025, 45(2): 0200004.
吕金光,梁静秋,赵百轩,等.干涉调制傅里叶变换光谱成像技术(特邀)[J].光学学报,2025,45(02):0200004.

[11] LV Jinguang, LIANG Jingqiu, ZHAO Baixuan, et al. Panoramic bispectral infrared imaging interference spectrum measurement inversion instrument[J]. Chinese Optics, 2022, 15(5): 1092-1104.
吕金光,梁静秋,赵百轩,等.全景双谱段红外成像干涉光谱测量反演仪器[J].中国光学(中英文),2022,15(5):1092-1104.

[12] WANG Chenfeng, WANG Xiaowei, LU Weiguo. Design of two-color cold infrared optical system[J]. Infrared and Laser Engineering, 2023, 52(12): 20230297.
王晨锋,王晓伟,陆卫国.双色低温红外光学系统设计[J].红外与激光工程,2023,52(12):20230297.

[13] BU Heyang, YU Linyao, TIAN Haonan, et al. Narcissus suppression of medium-wave infrared imaging system[J]. Chinese Optics, 2023, 16(6): 1414-1423.
卜和阳,虞林瑶,田浩南,等.中波红外成像系统冷反射抑制[J].中国光学(中英文), 2023, 16(6):1414-1423.

[14] LI Kang, ZHOU Feng, WANG Baohua, et al. Passive athermalization design of a cooled infrared optical system[J]. Chinese Optics, 2023, 16(4): 853-860.
李康,周峰,王保华,等.制冷型被动式消热差红外光学系统设计[J].中国光学(中英文),2023,16(4):853-860.
[15] CHEN Yupeng, LV Jinguang, WEI Yue, et al. A snapshot infrared imaging fourier transform spectrometer for dynamic target detection[J]. Remote Sensing, 2022, 7: 1543.
[16] ZHAO Baixuan. Data processing and performance evaluation of a tempo-spatially mixed modulation imaging Fourier transform spectrometer based on stepped micro-mirror[J]. Optics Express, 2020, 28.5: 6320-6335.

A Hybrid Refractive-diffractive Optical System Design for Mid-wave Infrared Interference Spectral Imaging

CHEN Yupeng[1,2], LIANG Jingqiu[1,2], LV Jinguang[1,2], ZHAO Baixuan[1,2], QIN Yuxin[1,2], ZHENG Kaifeng[1,2], ZHAO Yingze[1,2], NIE Haitao[1,2], WANG Weibiao[1]
(1 *Changchun Institute of Optics, Fine Mechanics and Physics, Chinese Academy of Sciences, Changchun* 130033, *China*)
(2 *State Key Laboratory of Advanced Manufacturing for Optical Systems, Changchun* 130033, *China*)

Abstract: Mid-wave infrared interference spectral imagers possess unique advantages in gas detection and identification due to their wide characteristic spectral coverage, high-throughput detection capability, and multi-channel sampling. Particularly in daily inspection and early warning of chemical gases and rapid emergency response to leakage scenarios, they can provide early warnings of disasters at the initial stage of gas leakage, preventing the situation from escalating. After a gas leak occurs, without requiring personnel to enter the site, they can quickly identify the type of leaking gas and the distribution of its diffusion concentration, providing first-hand on-site data for the evaluation of emergency response plans. However, traditional point-scan and area-scan interference spectral imaging configurations face significant limitations in enhancing lightweight, compact design, and stability. It is of great significance to research and design interference spectral imaging instruments that meet the high demands for mobility, adaptability to complex environments, field of view coverage, and lightweight compactness in specific application scenarios. Additionally, as interference spectral imagers require high precision in detector pixel intensity detection, it is necessary to study the analysis and suppression methods of infrared stray radiation in complex scenarios.

This paper proposes a spectral imaging system based on static interference modulation using a stepped micro-mirror. The optical configuration of the system is shown in Figure 1. The scanning telescope imaging lens assembly achieves wide-field one-time convergence imaging onto the stepped micro-mirror for interference modulation, and the image is then relayed onto the detection focal plane through the relay imaging lens group. A cylindrical design is introduced to compensate for the high-order astigmatism introduced by the interference beam-splitting system. Achromatic broadband design and athermalization across a wide temperature range are achieved through hybrid refractive-diffractive and aspheric designs, resulting in a static Modulation Transfer Function (MTF) better than 0.7 at the cutoff frequency. To analyze infrared stray radiation, a stray radiation model for the interference spectral imaging system was constructed. The materials and surface radiation scattering characteristics of the optomechanical structure were defined, and ray tracing was performed. Based on the tracing results, a stray radiation suppression structure was designed, achieving infrared radiation suppression at the level of 10^{-5}.

The telescope imaging lens group was optimized with an image-space telecentric design, while the relay imaging lens group adopted an object-space telecentric design, achieving a perfect match in a dual-high telecentric optical system. By employing hybrid refractive-diffractive and aspheric designs, the system demonstrated excellent performance in the mid-wave infrared band of 3 μm-5 μm across a temperature range of −40 ℃ to 60 ℃. The static MTF exceeded 0.7 at 17 lp/mm, distortion was controlled within 0.2%, and the RMS radius of the imaging spot was less than 5.9 μm, meeting all imaging quality requirements. A stray radiation simulation model for the interference spectral imaging optomechanical system, as illustrated in Figure 7, was constructed. Stray radiation tracing was performed for typical field light paths, and based on the analysis results, efficient suppression was achieved through blackbody

extinction treatment and dedicated stray radiation suppression structures. This reduced the infrared stray radiation energy ratio from an initial level of 10^{-2} to 10^{-5}. Imaging detection experiments on long-distance target scenes using an engineering prototype demonstrated excellent image quality. The MTF test of the prototype of high-precision alignment principle shows that the actual MTF of the designed imaging system is better than 0.32 at the cut-off frequency.

The infrared spectral imaging system based on static interference modulation with a stepped micro-mirror successfully achieves high-quality remote sensing imaging, identification and analysis of gases. The adoption of achromatic methods using cylindrical lenses and hybrid refractive-diffractive lenses, together with the stray radiation suppression method proposed in this paper, has all yielded the expected effects in optimizing imaging quality, which is proven to be effective and can serve as a reference for research in the same field. In addition, the instrument's volume is reduced by a quarter and its weight by approximately 60%, which also provides a valuable contribution to the miniaturization process of such imaging systems.

Key words: Optical design; Interference spectral imaging; Hybrid refractive-diffractive; Athermalization; Stray radiation suppression

OCIS Codes: 220.0220; 110.0110; 300.0300

CSTR: 32255.14.gzxb20265502.0222005

Foundation item: Natural Science Foundation of Jilin Provincial (20250102181JC), National Natural Science Foundation of China (62575282,62405317,62305339,62205332)